Journal of Statistical Physics, Vol. 100, Nos. 1/2, 2000

Analytic Approximations for the Velocity of Field-Driven Ising Interfaces

Per Arne Rikvold[1] **and M. Kolesik**[2, 3]

Received August 30, 1999; final November 24, 1999

We present analytic approximations for the field, temperature, and orientation dependences of the interface velocity in a two-dimensional kinetic Ising model in a nonzero field. The model, which has nonconserved order parameter, is useful for ferromagnets, ferroelectrics, and other systems undergoing order–disorder phase transformations driven by a bulk free-energy difference. The solid-on-solid (SOS) approximation for the microscopic surface structure is used to estimate mean spin-class populations, from which the mean interface velocity can be obtained for any specific single-spin-flip dynamic. This linear-response approximation remains accurate for higher temperatures than the single-step and polynuclear growth models, while it reduces to these in the appropriate low-temperature limits. The equilibrium SOS approximation is generalized by mean-field arguments to obtain field-dependent spin-class populations for moving interfaces, and thereby a nonlinear-response approximation for the velocity. The analytic results for the interface velocity and the spin-class populations are compared with Monte Carlo simulations. Excellent agreement is found in a wide range of field, temperature, and interface orientation.

KEY WORDS: Kinetic Ising model; solid-on-solid (SOS) approximation; microscopic interface structure; surface anisotropy; surface growth; interface dynamics; linear response; nonlinear response; Monte Carlo simulation.

[1] Center for Materials Research and Technology, School of Computational Science and Information Technology, and Department of Physics, Florida State University, Tallahassee, Florida 32306-4350; e-mail: rikvold@csit.fsu.edu.

[2] Institute of Physics, Slovak Academy of Sciences, Bratislava, Slovak Republic.

[3] Department of Mathematics, University of Arizona, Tucson, Arizona 85721; e-mail: kolesik@acms.arizona.edu.

0022-4715/00/0700-0377$18.00/0

1. INTRODUCTION

The appearance of the world around us through sight and touch is largely determined by interfaces between phases with different optical and mechanical properties, and the materials properties of multiphase media are strongly influenced by the geometry of interfaces that separate their constituent materials.[1, 2] Since, in general, the morphology of an interface is determined by the growth process by which it is formed, the large-scale structures of growing interfaces have inspired an enormous amount of work in the last few decades.[3, 4]

In comparison to the vigorous interest in large-scale structure, much less attention has been paid to interfacial structure on a microscopic scale. This is somewhat surprising since the microscopic structure limits the interfacial propagation velocity under an external driving force, such as the applied field for a magnetic or dielectric domain wall or the supersaturation or supercooling for a crystal surface. It is also important for properties such as chemical reactivity and catalytic activity.

In this paper we consider how the microscopic interface structure determines the growth velocity of a simple model surface in a system with nonconserved order parameter: the interface between domains of positive and negative magnetization in a square-lattice kinetic Ising ferromagnet with nearest-neighbor interactions, which is driven by a field favoring one of the two spin orientations.[5, 6, 7] This model is applicable to the kinetics of phase transformation in many magnetic and ferroelectric systems and other order-disorder transitions whose kinetics are not inhibited by coupling to a conserved field. It belongs to the dynamic universality class of the Kardar–Parisi–Zhang (KPZ) model,[8] and the velocity of a macroscopically plane interface is expected to be linear in an asymptotically weak field, as is also predicted by the Lifshitz–Allen–Cahn theory,[9, 10] However, neither theory gives the explicit field dependence, which should contain both the average interface orientation and the specific dynamic. Here we derive analytic, approximate expressions for the mean velocity as a function of field, temperature, and interface orientation. Our approach is based on the concept of *spin classes* used in rejection-free Monte Carlo (MC) algorithms,[11, 12, 13] together with the Burton–Cabrera–Frank solid-on-solid (SOS) approximation for the structure of a stationary interface.[14, 15] While the theory should become exact for asymptotically small temperatures and fields, our main purpose is to explore its applicability outside this limited regime.

The remainder of this paper is organized as follows. In Section 2 we introduce the kinetic Ising model and the concept of spin classes. In Section 3 we summarize relevant aspects of the SOS approximation for the

structure of a flat, equilibrium Ising interface between two bulk phases of opposite magnetization, which we use to obtain analytic approximations for the mean spin-class populations in zero field. These provide a linear-response approximation for the velocity of a driven interface. In Section 4 we develop an extension of the SOS approximation to obtain field-dependent spin-class populations for flat, moving interfaces as well. This leads to a nonlinear-response approximation for the velocity. In Section 5 the theoretical results for the interface velocity and spin-class populations from Sections 3 and 4 are compared with MC simulations. The nonlinear-response approximation gives remarkable agreement with the simulations in a wide range of field, temperature, and interface orientation. Section 6 contains a discussion, conclusions, and some suggestions for future work.

2. MODEL AND DYNAMICS

The anisotropic square-lattice Ising ferromagnet with nearest-neighbor interactions is defined by the Hamiltonian

$$\mathscr{H} = -\sum_{x,\,y} s_{x,\,y}(J_x s_{x+1,\,y} + J_y s_{x,\,y+1} + H) \tag{1}$$

Here $s_{x,\,y} = \pm 1$, $\sum_{x,\,y}$ runs over all lattice sites, and H is the applied field. The lattice constant is taken as our unit of length. An interface is introduced by fixing $s_{x,\,y} = +1$ and -1 for large negative and positive y, respectively. For concreteness we assume that $H \geqslant 0$, such that the interface moves in the positive y direction under an applied field. The implementation of these boundary conditions in our MC simulations is discussed in Section 5.1.

Approach to equilibrium is ensured by a single-spin-flip (nonconservative) dynamic which satisfies detailed balance, such as the Metropolis or Glauber algorithms.[16] Any such algorithm is defined by a transition probability, $W[s_{x,\,y} \to -s_{x,\,y}] = W[\beta \Delta E]$, where β is the inverse of the temperature T (we use units in which Boltzmann's constant is unity), and ΔE is the energy change that would occur if the proposed spin flip were accepted. Since there are only a finite number of different values of ΔE, the spins can be divided into classes,[6, 11] labeled by the spin value s and the number of broken bonds between the spin and its nearest neighbors in the x- and y-direction, j and k, respectively. The spin classes, denoted jks with $j, k \in \{0, 1, 2\}$, are listed in Table 1 together with the corresponding energies, $E(jks)$, and energy changes, $\Delta E(jks)$. For the anisotropic model

Table 1. Spin Classes in the Anisotropic Square-Lattice Ising Model[a]

Class, *jks*	$E(jks)-E_0$	$\Delta E(jks)$
$01s*$	$\pm H+2J_y$	$\mp 2H+4J_x$
$11s*$	$\pm H+2(J_x+J_y)$	$\mp 2H$
$21s*$	$\pm H+2(2J_x+J_y)$	$\mp 2H-4J_x$
$10s\dagger$	$\pm H+2J_x$	$\mp 2H+4J_y$
$20s\dagger$	$\pm H+4J_x$	$\mp 2H-4(J_x-J_y)$
$12s\ddagger$	$\pm H+2(J_x+2J_y)$	$\mp 2H-4J_y$
$02s\ddagger$	$\pm H+4J_y$	$\mp 2H+4(J_x-J_y)$
$22s$	$\pm H+4(J_x+J_y)$	$\mp 2H-4(J_x+J_y)$
$00s$	$\pm H$	$\mp 2H+4(J_x+J_y)$

[a] The first column gives the class labels, *jks*. The second column gives the total field and interaction energy for a spin in each class, $E(jks)$, relative to the energy of the state with all spins parallel and $H=0$, $E_0=-2(J_x+J_y)$. The third column gives the change in the total system energy that would result from reversing a spin in a particular class from s to $-s$, $\Delta E(jks)$. In both $E(jks)-E_0$ and $\Delta E(jks)$, the upper sign corresponds to $s=-1$, and the lower sign corresponds to $s=+1$. The first three classes (marked $*$) have nonzero populations in the SOS approximation, and flipping a spin in any of them preserves the SOS interface configuration. The next two classes (marked †) also have nonzero populations in the SOS approximation, but flipping a spin in any of them may produce an overhang or a bubble. The two classes marked ‡ have zero populations in the SOS approximation, but flipping a spin in any of them may lead to a configuration compatible with the SOS constraint. Class $22s$ represents a single spin which is antiparallel to all its neighbors; flipping such a spin yields a bulk spin in class $00-s$. Although only the classes marked $*$ and † have nonzero populations in the SOS approximation, the MC transition probabilities of all classes except $00s$ are given by Eq. (2). The bulk spins, $00s$, have zero transition probabilities in the dynamic used here.

defined by Eq. (1) there are 18 classes.[12] In the isotropic case, $J_x=J_y$, this reduces to 10 classes distinguished by s and the total number of broken bonds, $j+k$.[11]

For concreteness and comparison with numerical simulations we here choose the discrete-time Glauber dynamic, defined by the transition probability

$$W_{\mathrm{G}}[s_{x,y}\rightarrow -s_{x,y}]=\frac{e^{-\beta\Delta E}}{1+e^{-\beta\Delta E}} \tag{2}$$

The Glauber dynamic is mathematically convenient in that the transition probability is a continuously differentiable function of ΔE. In its continuum-time version it has also been shown to correspond to a quantum-mechanical $S=1/2$ system weakly coupled to a large thermal fermion

bath.[17] However, the spin-class populations can be used to estimate propagation velocities with any single-spin-flip dynamic that satisfies detailed balance. Time is measured in units of MC steps per spin (MCSS).

To prevent nucleation of droplets of the stable phase in front of the moving interface,[5] we modify the Glauber dynamic by setting the transition rate for any spin which is parallel to all its neighbors (i.e., class $00s$) equal to zero.[7, 18, 19] This suppresses thermal fluctuations in both the bulk phases, while the local interface structure is reasonably preserved. For moderate fields the interface velocity with this modified Glauber dynamic is only slightly less than that obtained with the full Glauber dynamic.[18, 19] In the strong-field regime, where the size of a critical droplet of the equilibrium phase is reduced to on the order of the lattice constant, the kinetic Ising interface loses its integrity. A conservative analytic approximation for this crossover field (often called "the mean-field spinodal"[20, 21]) is (for isotropic interactions)[22] $H_{\mathrm{MFSP}}(T) \approx \sigma(T)/m_{\mathrm{eq}}(T)$, where $\sigma(T)$ and $m_{\mathrm{eq}}(T)$ are the equilibrium surface tension in the x-direction and the equilibrium magnetization, respectively. In the strong-field regime the SOS approximation and the dynamic used here should be considered as a nonequilibrium cluster growth model in its own right. For $|H| < H_{\mathrm{MFSP}}(T)$ they constitute a good approximation for the kinetic Ising model with the full Glauber dynamic.[18, 19]

3. THE SOS APPROXIMATION

The separation of spins into classes forms the basis of several rejection-free MC algorithms.[11–13, 23–25] In such algorithms the spin-class populations, $n(jks)$, are continually monitored throughout the simulation. Given this information and the transition probabilities of the particular dynamic used, one can then calculate the time increments between MC updates. Here we instead obtain analytic approximations for the mean spin-class populations for a driven interface moving at a constant velocity, based on the Burton–Cabrera–Frank SOS model of the equilibrium interface.[14] These populations are then used together with the transition probabilities to obtain the mean interface velocity.

The SOS approximation describes the interface as a single-valued function $y(x)$. For the square lattice considered here, the interface is a series of integer-valued steps of height $\delta(x)$ parallel to the y-axis, as shown in Fig. 1. The heights of the individual steps are assumed to be statistically independent and identically distributed. The probability density function (pdf) is given by the interaction energy corresponding to the $|\delta(x)|$ broken

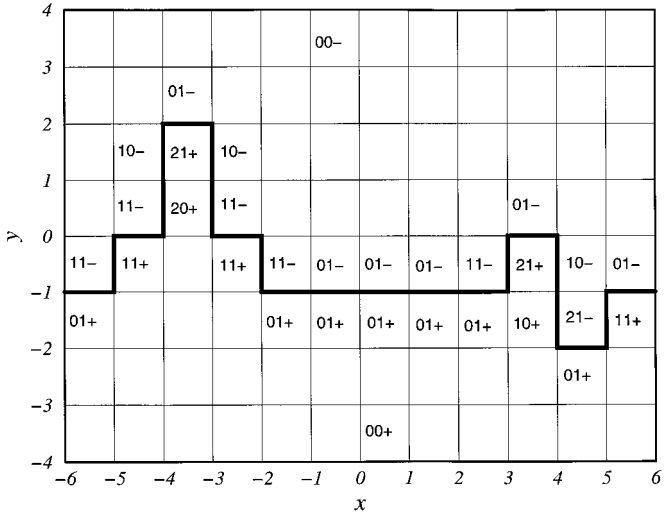

Fig. 1. A short segment of a zero-field equilibrium SOS interface between a positively magnetized phase for $y<0$ and a negative phase for $y>0$. The independent step heights, $\delta(x)$, are drawn from the pdf given by Eqs. (3) and (4) with $T=0.6T_c$ and $\phi=0$. Interface sites representative of the different spin classes compatible with the SOS approximation are marked with the notation *jks* explained in Section 2. Sites in the uniform bulk phases are $00-$ and $00+$.

J_x-bonds between spins in the columns centered at $(x-1/2)$ and $(x+1/2)$ as

$$p_x[\delta(x)] = Z_x^{-1} X^{|\delta(x)|} e^{\gamma(\phi)\,\delta(x)} \tag{3}$$

where we have introduced the shorthand $X=e^{-2\beta J_x}$. Here $\gamma(\phi)$ is a Lagrange multiplier which maintains the mean step height at an x-independent value, $\langle \delta(x) \rangle = \tan\phi$, where ϕ is the overall angle between the interface and the x-axis. The partition function is

$$Z_x = \sum_{\delta=-\infty}^{+\infty} X^{|\delta|} e^{\gamma(\phi)\,\delta} = \frac{1-X^2}{1-2X\cosh\gamma(\phi)+X^2} \tag{4}$$

Using Z_x as a moment generating function for $\delta(x)$, it is straightforward to obtain the explicit expression

$$e^{\gamma(\phi)} = \frac{(1+X^2)\tan\phi + R}{2X(1+\tan\phi)} \tag{5}$$

where $R=[(1-X^2)^2\tan^2\phi+4X^2]^{1/2}$. Combining Eqs. (4) and (5) one obtains Z_x explicitly as a function of ϕ:

$$Z_x(\phi)=\frac{(1-X^2)(1-\tan^2\phi)}{1+X^2-R} \tag{6}$$

For $\phi=0$ this simplifies to $Z_x(0)=(1+X)/(1-X)$. The SOS approximation ignores overhangs and bubbles. It is therefore rather remarkable that the surface tension in this approximation, calculated as $\sigma_{\mathrm{SOS}}=|\cos\phi|\,[2J_y-T\ln Z_x(\phi)+T\gamma(\phi)\tan\phi]$, yields the exact result for $\phi=0$[26] and an excellent approximation for $|\phi|\leqslant\pi/4$.[27] For larger $|\phi|$ it is more reasonable to use an SOS approximation with steps parallel to the x-axis.

While Eq. (6) is equivalent to Eq. (72) of ref. 14, the implicit form given by Eqs. (4) and (5) is more convenient for our purpose of obtaining mean spin-class populations, $\langle n(jks)\rangle$. The spin classes compatible with this approximation are illustrated in Fig. 1. The mean populations are all obtained from the joint pdf for $\delta(x)$ and $\delta(x+1)$. Since the individual step heights are statistically independent, this is the product $p_x[\delta(x)]\cdot p_{x+1}[\delta(x+1)]$. The symmetry of $p_x[\delta(x)]$ under the transformation $(x,\phi,\delta)\to(-x,-\phi,-\delta)$ ensures that $\langle n(jk-)\rangle=\langle n(jk+)\rangle$ for all j and k. (On the right-hand sides of Eqs. (7)–(10) below, we have chosen $s=-1$ with the interface oriented as shown in Fig. 1 for concreteness.)

The SOS picture implies that there is exactly one broken J_y bond per unit length in the x-direction, so that $\langle n(01s)\rangle+\langle n(11s)\rangle+\langle n(21s)\rangle=1$. The calculations of the individual populations are straightforward but somewhat tedious, especially for nonzero ϕ. In Eqs. (7)–(9) below we therefore just give the starting point of the calculation for each class in terms of $p_x[\delta(x)]$ and the cumulative probabilities $P[\delta(x)\leqslant n]=\sum_{\delta=-\infty}^{n}p_x(\delta)$ and $P[\delta(x)\geqslant n]=1-P[\delta(x)\leqslant(n-1)]$. The final results are listed in Table 2, both for general ϕ and for $\phi=0$.

$$\langle n(01s)\rangle=P[\delta(x)\geqslant 0]\cdot P[\delta(x+1)\leqslant 0] \tag{7}$$

$$\langle n(11s)\rangle=P[\delta(x)\leqslant -1]\cdot P[\delta(x+1)\leqslant 0]+P[\delta(x)\geqslant 0]\cdot P[\delta(x+1)\geqslant 1] \tag{8}$$

$$\langle n(21s)\rangle=P[\delta(x)\leqslant -1]\cdot P[\delta(x+1)\geqslant 1] \tag{9}$$

Flipping a spin in either of these classes (marked $*$ in Table 2) preserves the SOS configuration.

Table 2. The Mean Populations for the Spin Classes Included in the SOS Approximation, Together with Their Contributions to the Interface Velocity Under the Glauber Dynamic[a]

Class, jks	$\langle n(jks)\rangle$, general ϕ	$\langle n(jks)\rangle$, $\phi = 0$	$\langle v_y(jk)\rangle$
$01s*$	$\dfrac{1-2X\cosh\gamma(\phi)+X^2}{(1-X^2)^2}$	$\dfrac{1}{(1+X)^2}$	$\dfrac{\tanh(\beta H)}{1+[\sinh(2\beta J_x)/\cosh(\beta H)]^2}$
$11s*$	$\dfrac{2X[(1+X^2)\cosh\gamma(\phi)-2X]}{(1-X^2)^2}$	$\dfrac{2X}{(1+X)^2}$	$\tanh(\beta H)$
$21s*$	$\dfrac{X^2[1-2X\cosh\gamma(\phi)+X^2]}{(1-X^2)^2}$	$\dfrac{X^2}{(1+X)^2}$	$\dfrac{\tanh(\beta H)}{1+[\sinh(2\beta J_x)/\cosh(\beta H)]^2}$
$10s\dagger$	$\dfrac{2X^2}{1-X^2}\left\{\dfrac{2\cosh^2\gamma(\phi)-1-2X\cosh\gamma(\phi)+X^2}{1-2X\cosh\gamma(\phi)+X^2} - \dfrac{X^2[1-2X\cosh\gamma(\phi)+X^2]}{(1-X^2)^2}\right\}$	$\dfrac{2X^2(1+2X)}{(1-X^2)(1+X)^2}$	$\dfrac{\tanh(\beta H)}{1+[\sinh(2\beta J_y)/\cosh(\beta H)]^2}$
$20s\dagger$	$\dfrac{X^4[1-2X\cosh\gamma(\phi)+X^2]}{(1-X^2)^3}$	$\dfrac{X^4}{(1-X^2)(1+X)^2}$	$\dfrac{\tanh(\beta H)}{1+[\sinh[2\beta(J_x-J_y)]/\cosh(\beta H)]^2}$

[a] The first column gives the class labels, jks. The second column gives the mean spin-class populations for general tilt angle ϕ, with $\cosh\gamma(\phi)$ from Eq. (5). The third column gives the spin-class populations for $\phi = 0$. Using $X = e^{-2\beta J_x}$ in these expressions, one obtains the linear-response result in which the spin-class populations are evaluated for $H = 0$. Using $X = X(T, H)$ from Eq. (20) with the transition probabilities of the particular dynamic used [here: Glauber, Eq. (21)], one gets the nonlinear-response approximation, which includes an estimate of the field-dependent modifications of the spin-class populations in the moving interface. The fourth column contains the contributions to the mean interface velocity in the y-direction from spins in classes $jk-$ and $jk+$, using the Glauber dynamic. These are the only quantities in this table that depend explicitly on the specific dynamic, and they could easily be replaced with results for, e.g., Metropolis.

To obtain the mean populations for classes of spins that are connected to the interface only through one ($10s$) or two ($20s$) broken J_x bonds is more tedious. We found it most convenient first to calculate the joint pdf for $n = n(10s) + n(20s)$ and $n(20s)$:

$$p[n, n(20s)] = \begin{cases} P[\delta(x) \geqslant -1] \cdot P[\delta(x+1) \leqslant 1] & \text{for} \quad n = n(20s) = 0 \\ p_x[-(n+1)] \cdot P[\delta(x+1) \leqslant 1] + P[\delta(x) \geqslant -1] \cdot p_{x+1}[n+1] & \\ \qquad \text{for} \quad n \geqslant 1, \quad n(20s) = 0 & \\ p_x[-(n+1)] \cdot p_{x+1}[n(20s)+1] + p_x[-(n(20s)+1)] \cdot p_{x+1}[n+1] & \\ \qquad \text{for} \quad n > 1, \quad 1 \leqslant n(20s) < n & \\ p_x[-(n+1)] \cdot p_{x+1}[n+1] \qquad \text{for} \quad n(20s) = n \geqslant 1 & \end{cases} \tag{10}$$

The resulting expressions for $\langle n(10s) \rangle$ and $\langle n(20s) \rangle$ are marked † in Table 2. Flipping a spin in one of these classes results in the breaking of two J_y-bonds, and thus in the creation of an overhang or a bubble. The classes, $02s$, $12s$, and $22s$, are not populated in the SOS approximation, while $00s$ represents bulk sites which have zero transition rates with this dynamic.

Each column of the interface advances by one lattice constant in the y-direction whenever a spin flips from -1 to $+1$, regardless of its y-coordinate. Conversely, the interface recedes by one lattice constant whenever a spin flips from $+1$ to -1. The energy changes corresponding to a flip are given in the third column in Table 1. Since the spin-class populations on both sides of the interface are equal in this approximation, the contribution from sites in the classes $jk-$ and $jk+$ to the mean velocity in the y-direction is the difference between the transition probabilities for spin flips leading to advance and recession:

$$\langle v_y(jk) \rangle = W[\beta \Delta E(jk-)] - W[\beta \Delta E(jk+)] \tag{11}$$

The results corresponding to the Glauber transition probabilities from Eq. (2) are given in the last column in Table 2. (It is of course trivial to generalize to $\langle n(jk-) \rangle \neq \langle n(jk+) \rangle$, but this will not be needed here.) The mean propagation velocity perpendicular to the interface becomes

$$\langle v_\perp(T, H, \phi) \rangle = |\cos \phi| \sum_{j,k} \langle n(jks) \rangle \langle v_y(jk) \rangle \tag{12}$$

Including the SOS-violating moves, $jk \in \{10, 20\}$, in principle allows the propagation velocity to exceed unity as it becomes possible to flip several spins along a high vertical step. However, such large velocities are only observed for the strongest fields investigated here. Restricting the sum to only $jk \in \{01, 11, 21\}$, on the other hand, yields an approximation which excludes SOS-violating transitions and would limit the velocity to below unity.

While the general result for the velocity is rather cumbersome if written out in detail, the special case of $\phi = 0$ leads to a relatively compact formula:

$$\begin{aligned}\langle v_\perp(T, H, 0)\rangle = \frac{\tanh(\beta H)}{(1+X)^2}\Bigg\{2X + \frac{1+X^2}{1+[\sinh(2\beta J_x)/\cosh(\beta H)]^2} \\ + \frac{X^2}{1-X^2}\Bigg[\frac{X^2}{1+[\sinh(2\beta(J_y-J_x))/\cosh(\beta H)]^2} \\ + \frac{2(1+2X)}{1+[\sinh(2\beta J_y)/\cosh(\beta H)]^2}\Bigg]\Bigg\}\end{aligned} \tag{13}$$

Here the first line corresponds to transitions that preserve the SOS structure of the interface, while the next two lines correspond to transitions that create overhangs or bubbles. Comparison with simulation data indicate that excluding the SOS-violating transitions leads to significant underestimation of the propagation velocity, even for quite moderate fields. This effect is shown in Fig. 2 and discussed in more detail in Section 5.2.

Equation (13) with $J_x = J_y$ was presented without detailed derivation in ref. 19. In that work the average interface velocity in a kinetic Ising model undergoing a field-driven phase transformation was estimated directly from the time evolution of the magnetization after a sudden field reversal. This estimate was found to be consistent with Eq. (13).

As $T \to 0$, $X \to 0$. In this limit, the dominant term in Eq. (12) is the one proportional to $\langle n(11s)\rangle$, which is simply the density of kinks on the surface. Combining the appropriate entries in Table 2 with Eq. (5) and ignoring X everywhere except where X^2 occurs in an additive combination with $\tan^2\phi$, we get the angle-dependent interface velocity for very low T:

$$\langle v_\perp(T \to 0, H, \phi)\rangle = \cos\phi\,\frac{\sqrt{\tan^2\phi + 4X^2} - \tan^2\phi}{1 - \tan^2\phi}\tanh(\beta H) \tag{14}$$

$$\approx \begin{cases}\dfrac{1}{2}\dfrac{|\sin 2\phi|}{|\sin\phi| + |\cos\phi|}\tanh(\beta H) & \text{for} \quad \tan\phi \gg X \\ \sqrt{\tan^2\phi + 4X^2}\tanh(\beta H) & \text{for} \quad \tan\phi \ll X\end{cases} \tag{15}$$

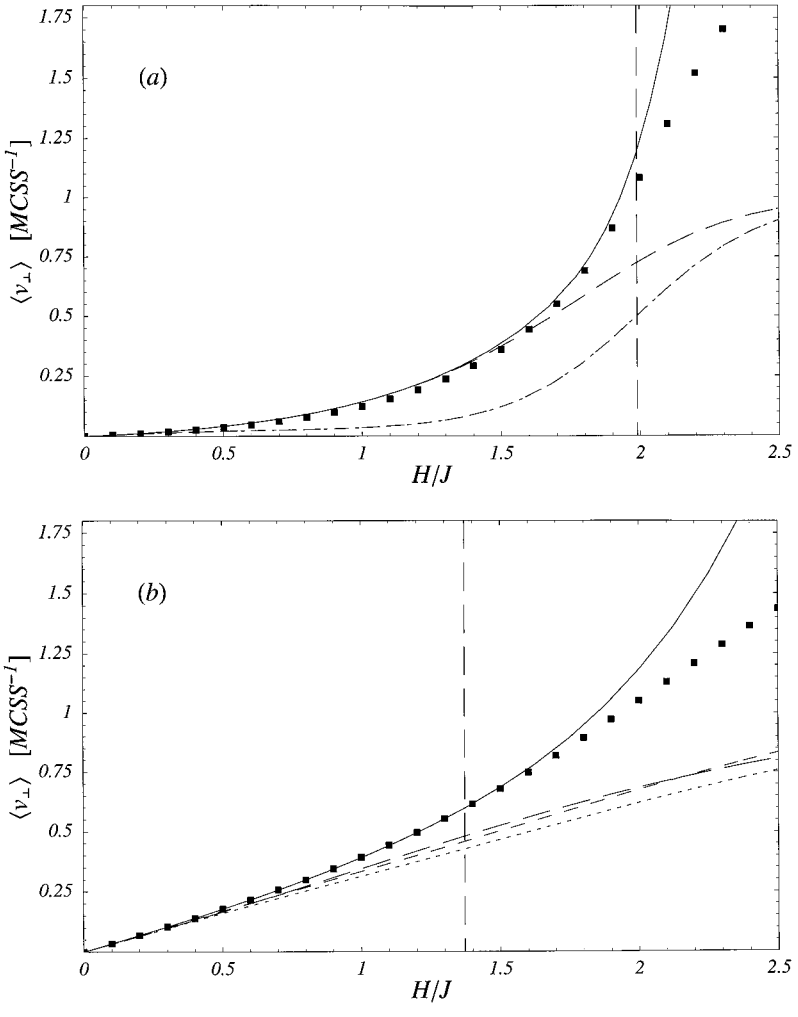

Fig. 2. Comparison between MC simulations and the four different analytic approximations introduced here. Shown is the normal interface velocity $\langle v_\perp \rangle$ vs H for $\phi = 0$ at $T = 0.2T_c$ (a) and $T = 0.6T_c$ (b). MC data (squares), linear-response excluding SOS-violating transitions (dotted), linear-response including SOS-violating transitions (short-dashed), nonlinear-response excluding SOS-violating transitions (long-dashed), and nonlinear-response including SOS-violating transitions (NLI) (solid). In the low-temperature case shown in (a) the two linear-response approximations are almost indistinguishable, and the dotted and short-dashed curves coincide as the lowest of the three curves shown. Statistical errors in the MC data are everywhere much smaller than the symbol size, both in this and all subsequent figures. The vertical long-dashed lines mark the crossover field $H_{\mathrm{MFSP}}(T)$. In both (a) and (b), the NLI approximation gives the best overall agreement with the data. It is the only one which will be used in subsequent figures.

The first line of Eq. (15) corresponds to the single-step model.[5, 6, 28, 29] In ref. 6 the same result was obtained from a Green–Kubo-like linear-response formula for the interface mobility. In the second line we retain only those terms in $\tan^2\phi$, which dominate in the limit $|\tan\phi| \ll X$, $X \to 0$. It corresponds to the polynuclear growth (PNG) model.[5, 30, 31] Equation (14) provides a correct interpolation between the PNG and single-step results as $|\tan\phi|$ increases from $|\tan\phi| \ll X$ to $|\tan\phi| \gg X$. Only the factor $\tanh(\beta H)$, which corresponds to the average velocity of a single step along the surface, depends explicitly on the specific dynamic. At higher temperatures than those for which Eq. (14) holds, the other spin classes contribute to the interface velocity as well, and our approximation goes beyond the single-step and PNG approximations.

4. NONLINEAR-RESPONSE SOS APPROXIMATION

The velocity estimates obtained in Section 3 were derived from the equilibrium interface fluctuations at $H = 0$ and thus constitute a linear-response approximation. This is satisfactory for sufficiently weak fields. For stronger fields, however, the structure of the moving interface is, in general, modified, leading to additional field dependences in the velocity. As will be shown in Section 5, this effect can be significant. In this section we therefore develop a mean-field theory for the step-height pdf for a moving, flat SOS interface in a nonzero field.

The step-height pdf for a *stationary* SOS interface in a *nonzero* field is[14]

$$p_x[\delta(x)] = Z_x^{-1} X^{|\delta(x)|} e^{[\gamma(\phi) - 2\beta H x]\,\delta(x)} \tag{16}$$

The term containing H adds an x-dependence to the Lagrange multiplier which determines $\langle \delta(x) \rangle$. The corresponding x-dependence in the partition function is obtained by replacing $\gamma(\phi)$ by $[\gamma(\phi) - 2\beta H x]$ in Eq. (4), where now $\tan\phi = \langle \delta(0) \rangle$. The geometric structure described by Eq. (16) is a macroscopically curved interface which bulges in the direction of the metastable phase region. For the case of conserved order parameter or nonconserved order parameter with an interface pinned at two points, the stationary configuration is an equilibrium one. For nonconserved order parameter without pinning, it corresponds to a critical droplet of the stable phase. If the average curvature is changed from the x-dependent form given by Eq. (16), the interface will move.

It is well known that the macroscopic, stationary distribution for flat, moving interfaces in the KPZ universality class is Gaussian,[3, 8] corresponding to a random walk with independent increments. Nevertheless, the step heights in several discrete models in this class are known to be

correlated at *short* distances.[32, 33] Here we develop a mean-field theory for the single-step-height pdf of the moving interface by ignoring these short-range correlations. Thus we assume that the step heights are statistically independent and identically distributed, just as they are for $H=0$. In this approximation, the single-step pdf of a moving interface parallel to the x-axis is given by Eqs. (3) and (4) with $\gamma=0$ and an H-dependent generalization of the parameter X. We now construct a self-consistency equation to determine this parameter, $X(T, H)$.

For simplicity we consider the step at $x=0$, and we take $\delta(0)\geqslant 0$. The equations obtained by considering other values of x and $\delta(x)\leqslant 0$ are identical to the one we derive below. The total transition probability for the height of a single step to change from δ to $\delta\pm 1$ is $\mathscr{W}[\delta\to\delta\pm 1]$. Relating the single-step transition probability to the single-step-height pdf by detailed balance, we have:

$$X(T, H)\equiv\frac{p_0[\delta(0)+1]}{p_0[\delta(0)]}=\frac{\mathscr{W}[\delta(0)\to\delta(0)+1]}{\mathscr{W}[\delta(0)+1\to\delta(0)]} \tag{17}$$

To find these transition probabilities, we refer to Fig. 3. In order for $\delta(0)$ to increase by one, either the spin at $x=+1/2$ can flip from -1 to $+1$, decreasing $\delta(+1)$ by one, or the spin at $x=-1/2$ can flip from $+1$ to -1, decreasing $\delta(-1)$ by one. Each of these possibilities is attempted with probability 1/2. For each spin-flip direction, the resulting energy change can have two different values, depending on the height of the corresponding neighboring step. Analogous arguments hold for the reverse transitions, $\delta(0)+1\to\delta(0)$. The energy changes and the conditions on the neighboring step heights are given next to the arrows denoting the directions of the transitions in Fig. 3. Expressing the single-spin transition rate corresponding to an energy change ΔE as $W[\Delta E]$ and reading the energy changes and conditions off from Fig. 3, we get:

$$\begin{aligned}
\mathscr{W}[\delta(0)\to\delta(0)+1]=\tfrac{1}{2}\{&W[-2H]\,P[\delta(+1)\geqslant +1]\\
&+W[-2H+4J_x]\,P[\delta(+1)\leqslant 0]\\
&+W[+2H]\,P[\delta(-1)\geqslant +1]\\
&+W[+2H+4J_x]\,P[\delta(-1)\leqslant 0]\}\\
\mathscr{W}[\delta(0)+1\to\delta(0)]=\tfrac{1}{2}\{&W[+2H]\,P[\delta(+1)\geqslant 0]\\
&+W[+2H-4J_x]\,P[\delta(+1)\leqslant -1]\\
&+W[-2H]\,P[\delta(-1)\geqslant 0]\\
&+W[-2H-4J_x]\,P[\delta(-1)\leqslant -1]\}
\end{aligned} \tag{18}$$

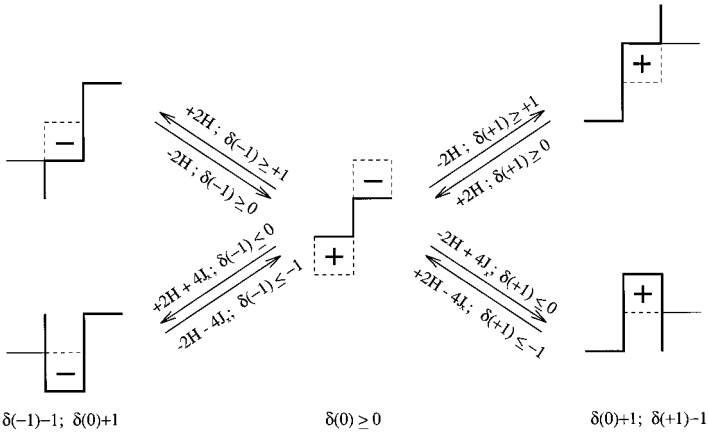

Fig. 3. Figure for calculating the transition rates $\mathscr{W}[\delta(0) \to \delta(0)+1]$ and $\mathscr{W}[\delta(0)+1 \to \delta(0)]$, Eq. (18). Interface configurations are indicated by bold line segments. Like in Fig. 1, the negatively magnetized phase is above the interface, and the positively magnetized phase below it. At the center is shown a step $\delta(0) \geqslant +1$ (here shown as $\delta(0) = +1$ for concreteness). A transition to $(\delta(0)+1)$ can be effected by flipping either one of the spins in the dashed boxes, each with probability 1/2. Flipping the initially negative spin $(-)$ decreases $\delta(+1)$ by one. The resulting configurations are shown to the right. The energy change depends on the initial value of $\delta(+1)$, and the two possible energy changes and the corresponding conditions are shown next to the right-pointing arrows. The thin horizontal lines represent the interface configuration corresponding to the equality in the conditions. The energy changes and conditions for the reverse transitions are shown next to the left-pointing arrows. Flipping the initially positive spin $(+)$ analogously decreases $\delta(-1)$ by one. The energy changes and conditions for the forward and reverse transitions resulting from flipping this spin, are indicated in the left-hand half of the figure.

Consistent with the mean-field approximation we calculate the cumulative probabilities with the same stationary single-step pdf, obtaining $P[\delta \geqslant 0] = P[\delta \leqslant 0] = 1/[1+X(T,H)]$ and $P[\delta \geqslant +1] = P[\delta \leqslant -1] = X(T,H)/[1+X(T,H)]$. The resulting self-consistency equation for $X(T,H)$ is

$$X(T,H) = \frac{\begin{array}{c} X(T,H)\{W[-2H]+W[+2H]\} \\ +W[-2H+4J_x]+W[+2H-4J_x] \end{array}}{\begin{array}{c} W[-2H]+W[+2H] \\ +X(T,H)\{W[-2H-4J_x]+W[+2H-4J_x]\} \end{array}} \tag{19}$$

This is solved to yield

$$X(T,H) = e^{-2\beta J_x}\left\{\frac{e^{-2\beta H}W[-2H-4J_x]+e^{2\beta H}W[+2H-4J_x]}{W[-2H-4J_x]+W[+2H-4J_x]}\right\}^{1/2} \tag{20}$$

where we have also used the detailed-balance relation for the single-spin transition probabilities, $W[+\Delta E]/W[-\Delta E] = e^{-\beta \Delta E}$, to eliminate $W[+2H+4J_x]$ and $W[-2H+4J_x]$.

The approach described above is also applicable to curved interfaces, and the resulting self-consistency equations are cubic in $X(T, H)$. However, except for the stationary curved interface described by Eq. (16), the shapes of such interfaces are not stationary and much more difficult to investigate by simulations. We hope to return to these more complicated problems in the future.

Equation (20) shows that $X(T, H)$ depends on the specific dynamic, except for $H = 0$, where it reduces to its equilibrium value, $X(T, 0) = e^{-2\beta J_x}$, for all dynamics that satisfy detailed balance.

Using the Glauber dynamic defined by Eq. (2), we get explicitly

$$X_{\mathrm{G}}(T, H) = e^{-2\beta J_x} \left\{ \frac{e^{2\beta J_x} \cosh(2\beta H) + e^{-2\beta J_x}}{e^{-2\beta J_x} \cosh(2\beta H) + e^{2\beta J_x}} \right\}^{1/2} \tag{21}$$

The Metropolis dynamic, $W_{\mathrm{M}}[\Delta E] = \min[1, e^{-\beta \Delta E}]$, yields

$$X_{\mathrm{M}}(T, H) = \begin{cases} e^{-2\beta J_x} \{\cosh(2\beta H)\}^{1/2} & \text{for} \quad H \leqslant 2J_x \\ \left\{ \dfrac{1 + e^{-\beta(2H+4J_x)}}{e^{-\beta(2H-4J_x)} + 1} \right\}^{1/2} & \text{for} \quad H \geqslant 2J_x \end{cases} \tag{22}$$

Numerically, X_{G} and X_{M} are not very different, and they both approach unity from below as H increases beyond $2J_x$. They are shown together vs H in Fig. 4.

The approximation used in ref. 19, $X(T, H) = e^{-2\beta J_x} \cosh(\beta H)$, can be obtained by "brutally decoupling" the steps through fictitiously splitting each spin in two and flipping only half of a spin to change the height of a single step. For such a process Eq. (17) directly yields $X(T, H) = \{W[-H+2J_x] + W[+H+2J_x]\} / \{W[+H-2J_x] + W[-H-2J_x]\}$, from which the result in ref. 19 is obtained for $H < 2J_x$ using the Metropolis dynamic. It is surprisingly close to the proper mean-field results and is included in Fig. 4 for comparison.

In their study of a lattice-gas model for three-dimensional crystal growth,[34] Kotrla and Levi introduced a single-site dynamic which in Ising language can be described (up to an overall rate factor $e^{2\beta H}$) as the product of Metropolis for field effects and Glauber for interaction effects: $W_{\mathrm{KL}}[-2H-4J_x] = W_{\mathrm{G}}[-4J_x]$ and $W_{\mathrm{KL}}[+2H-4J_x] = e^{-2\beta H} W_{\mathrm{G}}[-4J_x]$. Inserting these transition probabilities in Eq. (20), one finds that they lead to an H-independent X. This is indeed the case for any dynamic in which the field and interaction effects are statistically independent and

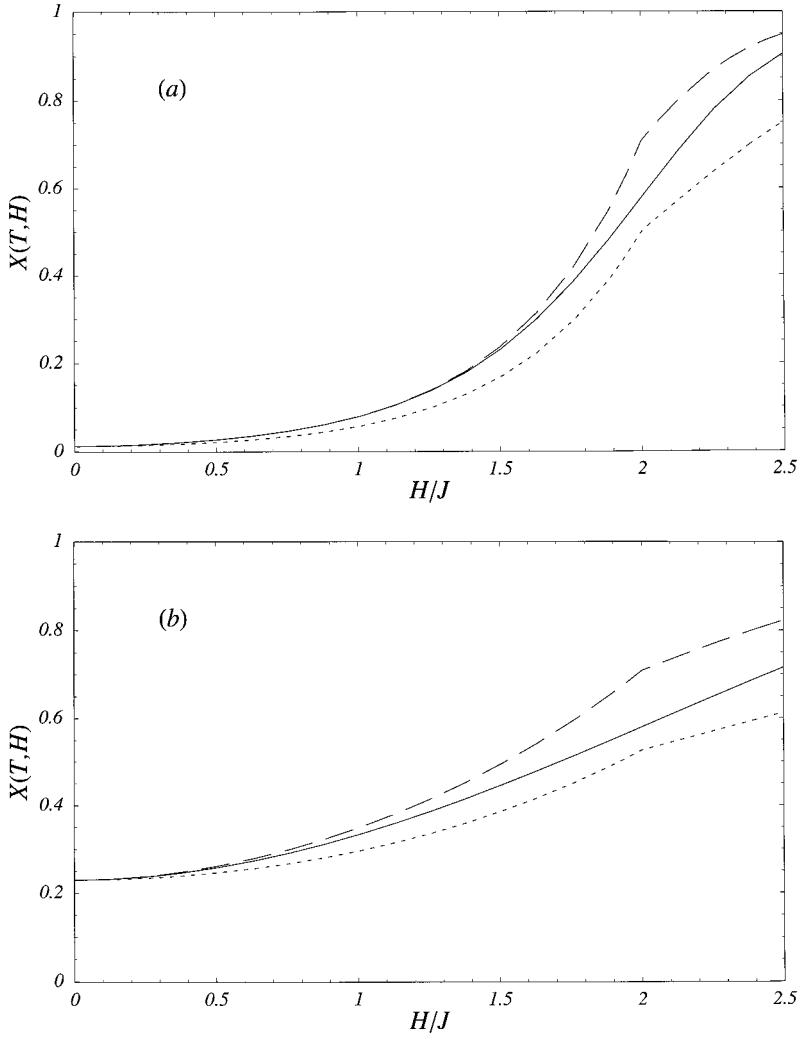

Fig. 4. The parameter $X(T, H)$ for different dynamics, shown vs H at $T = 0.2T_c$ (a) and $T = 0.6T_c$ (b). Solid curves: Glauber dynamic, $X_G(T, H)$, Eq. (21). Long-dashed curves: Metropolis dynamic, $X_M(T, H)$, Eq. (22). Dotted curves: The approximation used in ref. 19.

obey detailed balance separately. It shows that the local interface structure of driven interfaces can vary strongly as the dynamics are changed, even within the class of nonconservative single-spin-flip dynamics. Dynamics that factorize in this way are known as "soft," in contrast to the "hard" dynamics which do not factorize, such as Metropolis and the Glauber rate

used here. Soft and hard dynamics have been shown to lead to differences in the steady states in a number of other nonequilibrium systems as well.[35]

All the results for the spin-class populations of the zero-field equilibrium interface, which were derived in Section 3 and are listed in Table 2, can now be applied to obtain a nonlinear-response approximation for the propagation velocity of flat, driven interfaces. This simply requires replacing the zero-field $X = e^{-2\beta J_x}$ used in the linear-response approximation by the field-dependent $X(T, H)$, obtained from Eq. (20) with the transition probabilities corresponding to the particular dynamic used. For most hard dynamics, the net effect is to increase the mean step height, $\langle |\delta| \rangle$, and thus the interface velocity.

In the next section we show that this nonlinear-response approximation gives good agreement with MC simulations of driven, flat Ising interfaces for a wide range of fields and temperatures.

5. COMPARISON WITH MONTE CARLO SIMULATIONS

We have compared the analytical estimates of propagation velocities and spin-class populations developed above with MC simulations of the same model for $J_x = J_y = J$.

5.1. Simulation Details

To minimize the finite-size effects (see below), large simulation lattices are needed to accommodate a sufficient length of the interface and provide enough room for it to move unimpeded. To achieve long simulation runs it is necessary to employ a co-moving simulation box to prevent the interface from hitting the system boundary in the y-direction. We therefore used an "active-zone" algorithm which relies on the fact that spins with no broken bonds have zero transition probability. The algorithm uses a lattice of size L_x in the x-direction, and it keeps a list of all spins which have at least one broken bond and thus can flip in the next simulation step. Once a spin loses its last broken bond, it is removed from the "active list." A new spin is added to the list as soon as it acquires a broken bond due to a transition of one of its neighbors. The memory required for the list is proportional to the length of the interface, $L_x/|\cos\phi|$. No lattice boundaries are needed in the y-direction, and consequently arbitrarily long simulation runs can be performed. Except for these modifications, the algorithm is a straightforward implementation of the discrete-time n-fold way.[11]

The mean tilt angle ϕ was fixed by helical boundary conditions in the x-direction. The production runs were performed with $L_x = 1000$ and fixed ϕ between 0 and $\pi/4$. Since kinetic Ising interfaces belong to the KPZ universality class,[5, 8] the macroscopic interface width, $\langle [\, y(x,t) - \langle\, y(x,t) \rangle\,]^2 \rangle^{1/2}$, is expected to saturate at a value proportional to $L_x^{1/2}$ after a time $t \propto L_x^{3/2}$. In order to ensure stationarity we ran the simulation for 10 000 MCSS before taking any measurements. Exploratory runs with both larger and smaller L_x and "warm-up" times showed that the values used in the production runs were sufficient to ensure a macroscopically stationary interface. Class populations and interface velocities were averaged over 200 000 MCSS. The macroscopic stationarity of the interface should abundantly ensure the stationarity of these quantities, which are properties of the *local* interface structure.

5.2. Interface Velocities

The overall quality of the four different approximations developed above (linear-response (Section 3) and nonlinear-response (Section 4), each either excluding or including the SOS-violating transitions from classes $10s$ and $20s$) were explored in a wide range of H and T. In Fig. 2 the four approximations are compared with MC data for interfaces parallel to the x-axis at $T = 0.2T_c$ [Fig. 2(a)] and $T = 0.6T_c$ [Fig. 2(b)], where T_c is the exact critical temperature. The crossover field $H_{\mathrm{MFSP}}(T)$ is marked by a vertical dashed line in both (a) and (b). At the lowest temperature, the interface has very few steps higher than one for $H = 0$. As a result, it makes practically no difference whether SOS-violating transitions are allowed or not, and the curves representing the linear-response approximations including and excluding SOS-violating transitions coincide in Fig. 2(a). The nonzero field increases the average step height, and as a result the SOS-violating transitions contribute significantly for stronger fields in the nonlinear-response approximation. Overall, the nonlinear-response approximation including SOS-violating transitions ("nonlinear inclusive" or NLI) is everywhere better than the others and is particularly good for $H < H_{\mathrm{MFSP}}(T)$. It is the only one which will be used in the rest of this paper.

The temperature dependence between $T = 0$ and T_c of the velocities of interfaces parallel to the x-axis are shown in Fig. 5 for several values of H/J between 0.2 and 2.0. For $H/J \leqslant 1.5$, the discrepancy is nowhere greater than a few percent—mostly much smaller. Even for $H/J = 1.9$ and 2.0, the discrepancy remains below about 15% everywhere.

The anisotropy of the interface velocities is shown in Fig. 6 for several values of H/J between 0.1 and 2.0. The agreement between the NLI

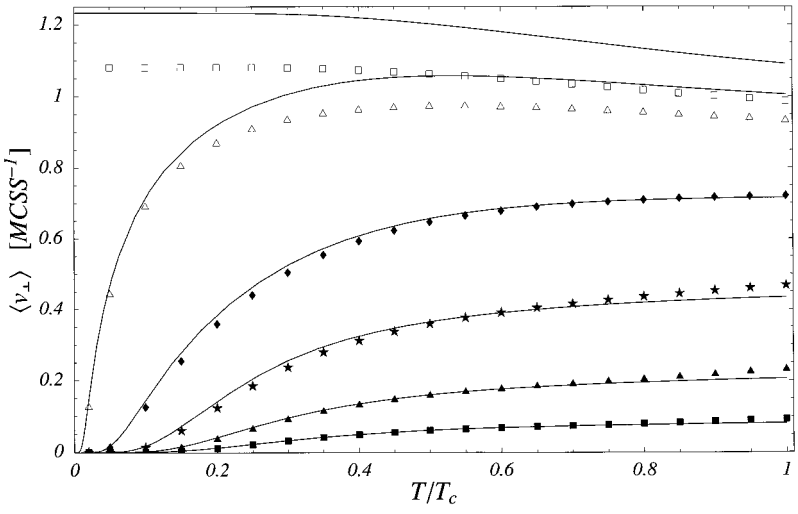

Fig. 5. Temperature dependence of the normal interface velocity, $\langle v_\perp \rangle$, for $\phi = 0$ at $H/J = 2.0$, 1.9, 1.5, 1.0, 0.5, and 0.2 from top to bottom. MC simulations (data points) and the NLI analytic approximation (solid curves).

approximation and the simulations is very good, except for the strongest fields. At $T = 0.2T_c$ [Fig. 6(a)], both the analytic and simulation results for $H/J \leqslant 1.5$ increase with increasing ϕ. As predicted by Eqs. (14) and (15), under weak fields they cross over from the form of the PNG model for $\tan\phi \ll X$, to almost exact agreement with the single-step model for $\tan\phi \gg X$ [Fig. 6(b)]. Growth shapes generated from these velocities would be almost square, with their sides parallel to the x and y axes.[5] For strong fields, however, the analytic approximation predicts velocities that are slightly larger in the symmetry directions than for inclined interfaces, as is the case for the Eden model.[36–38] This reverse anisotropy is not seen in the MC data, which become almost perfectly isotropic and would lead to circular growth shapes. With the Glauber dynamic it appears that stronger fields and lower temperatures are needed to observe reverse anisotropy in the MC data.[5] However, the discrepancies between the simulations and the analytic approximation are modest in the regime explored here, even near $\phi = \pi/4$ for strong fields. For small ϕ the agreement remains good for all fields $H/J \leqslant 1.9$. At $T = 0.6T_c$ [Fig. 6(c)], the simulated velocities are practically isotropic for all fields. The analytic NLI approximation works well, except for gradually increasing Eden-like reverse anisotropy for the stronger fields.

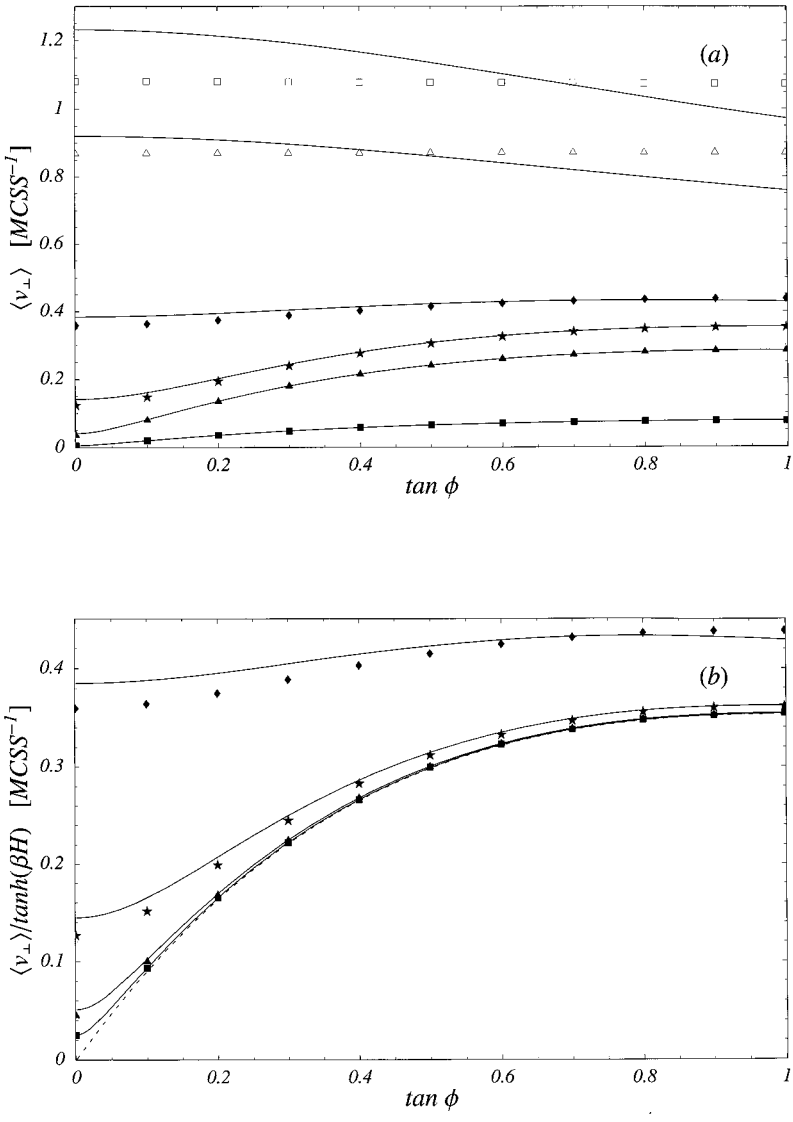

Fig. 6. The normal interface velocity $\langle v_\perp \rangle$, shown vs $\tan\phi$ for different fields. Simulation data are shown as data points and the NLI approximation as solid curves. The fields included are (from top to bottom) $H/J = 2.0$ (empty squares, only in a and c), 1.9 (empty triangles, only in a), 1.5 (filled diamonds), 1.0 (filled stars), 0.5 (filled triangles), and 0.1 (filled squares). (a) At $T = 0.2T_c$. (b) The four weakest fields at $T = 0.2T_c$, divided by $\tanh(\beta H)$. This shows the crossover between PNG and single-step growth, Eqs. (14) and (15). The dotted curve is the zero-temperature single-step result. (c) At $T = 0.6T_c$.

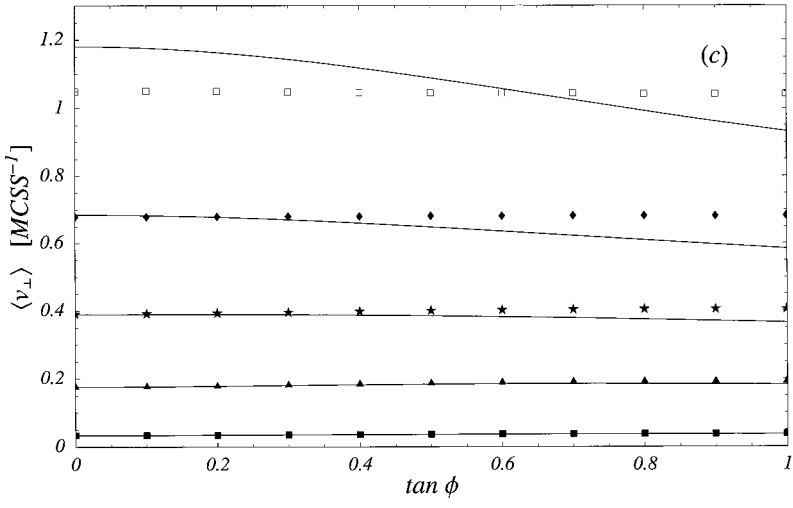

Fig. 6. (*Continued*)

5.3. Spin-Class Populations

While our main emphasis is on estimates of the interface velocity, the most detailed information about the strengths and weaknesses of our mean-field approximation for the interface structure is found in the individual spin-class populations. Examples of the H-dependences for $\phi = 0$ at $T = 0.6T_c$ are shown in Fig. 7. Individual populations are shown in Figs. 7(a) and (b), while spin classes with the same number of broken bonds are combined in Fig. 7(c). The crossover field $H_{\mathrm{MFSP}}(T)$ is shown in all three panels as a vertical dashed line. The agreement between the theoretical estimates and the MC data is good out to about this field.

The discrepancies that develop with increasing H stem from two sources. One is the fact that the simulated interface, unlike the SOS description used in the theoretical analysis, is not restricted to be free of overhangs and bubbles. The other is the development of correlations between neighboring step heights, which are not included in our single-step mean-field theory for the local structure of the driven SOS interface.

The presence of overhangs and bubbles is clearly reflected in the increase of $\langle n(01s) \rangle$, relative to the monotonically decreasing analytic approximation [Fig. 7(a)], and in the nonzero populations of the classes that are not populated in the SOS approximation [Fig. 7(b)].

The increasing correlations between nearest-neighbor steps is expressed by the gradual disappearance of the symmetry between the populations of

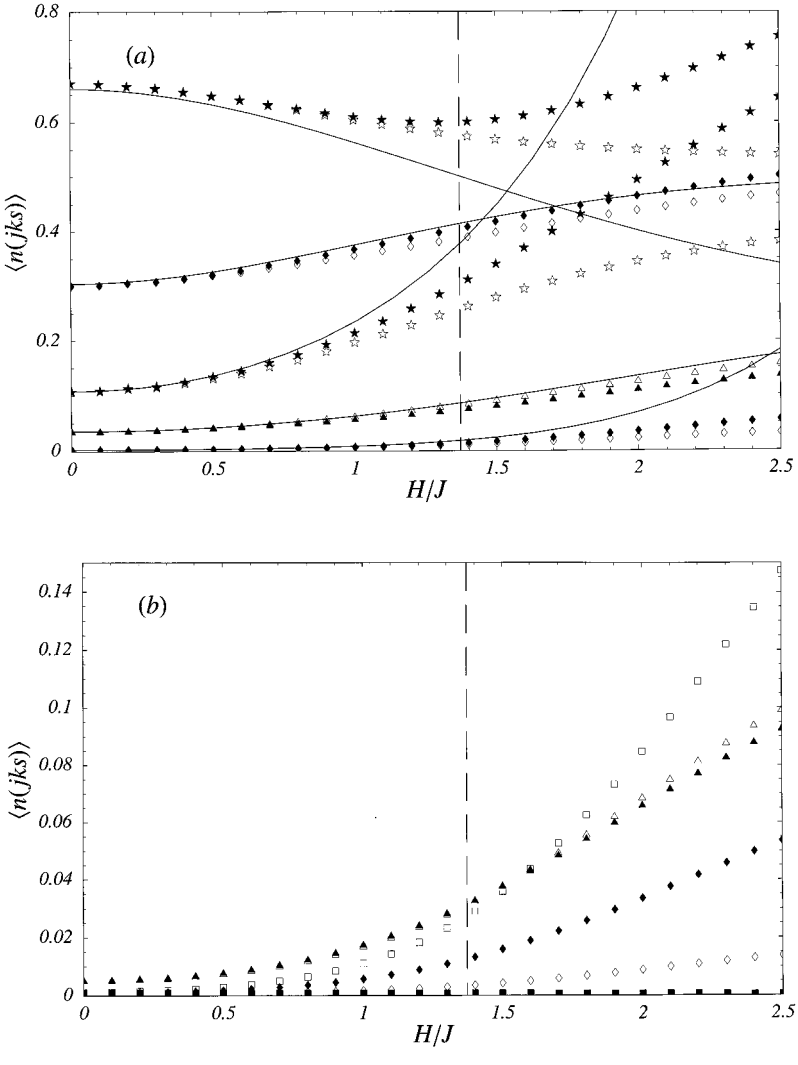

Fig. 7. Comparison between MC simulations (filled symbols for $s=+1$ and empty symbols for $s=-1$) and the NLI analytic approximation (solid curves) for the spin-class populations. Results for $T=0.6T_c$ and $\phi=0$ are shown vs H. (a) Individual populations of the spin classes compatible with the SOS picture. From top to bottom in the left part of the figure are $01s$ (stars), $11s$ (diamonds), $10s$ (stars), $21s$ (triangles), and $20s$ (diamonds). (b) Individual populations of the spin classes that would be unpopulated for a perfect SOS surface: $02s$ (diamonds), $12s$ (triangles), and $22s$ (squares). These nonzero populations clearly indicate the gradual breakdown of the SOS approximation with increasing H. (c) Class populations combined according to number of broken bonds, $j+k$. From top to bottom: one (stars), two (diamonds), three (triangles), and four (squares) broken bonds.

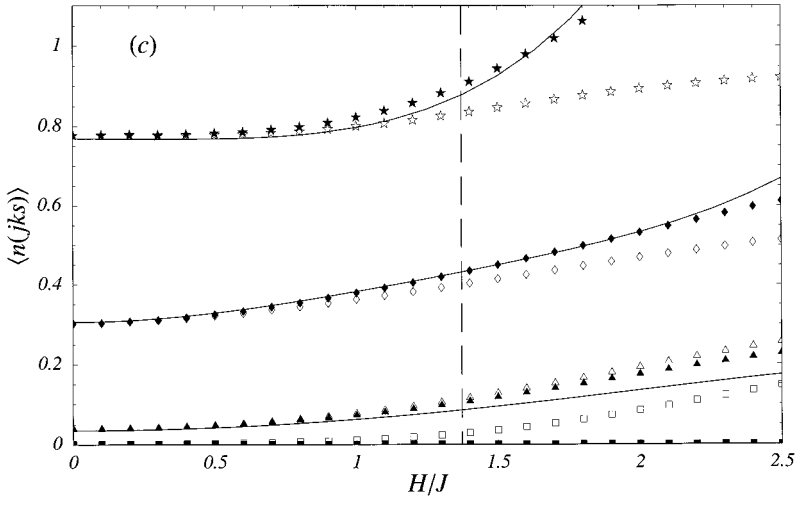

Fig. 7. (*Continued*)

spins with $s=+1$ (stable) and $s=-1$ (unstable) as the field is increased. The effect of these correlations is typically to broaden protrusions on the leading side of the interface ("hilltops") and sharpen protrusions on the trailing side ("valley bottoms"),[32] or *vice versa*.[33] In terms of spin-class populations, the former corresponds to $\langle n(21+)\rangle < \langle n(21-)\rangle$ and $\langle n(11+)\rangle > \langle n(11-)\rangle$. This is precisely what is seen in the simulations [Fig. 7(a)]. More generally, we find that the populations of $s=+1$ are enhanced for the classes with one and two broken bonds, while the populations of $s=-1$ are enhanced for the classes with three and four broken bonds [Fig. 7(c)]. The latter include both sharp valley bottoms and bubbles of the unstable phase, which form a wake behind the moving interface. This shows that the breakdown of the SOS description and the evolution of lateral correlations are not independent at strong fields. The overall picture is essentially the same at $T=0.2T_c$: both the populations in the non-SOS classes, and the asymmetry become significant only near $H_{\mathrm{MFSP}}(T)$, which at that temperature is close to $H/J=2$.

6. DISCUSSION

In this paper we introduced and explored analytic approximations for the propagation velocity and spin-class populations of a field-driven

interface in a two-dimensional kinetic Ising model. The model is applicable to a number of systems undergoing order-disorder phase transformations, including magnetic and ferroelectric systems and crystal growth under conditions which are not limited by diffusion.

The approximations are based on a linear-response approach, in which the equilibrium fluctuations of the interface (as embodied in average spin-class populations) were estimated from the Burton–Cabrera–Frank SOS model. The theory was extended by developing a mean-field approximation for the field-dependent spin-class populations in a moving flat interface, yielding a nonlinear-response approximation for the interface velocity. This extension considerably improves the agreement with MC simulations.

Our simulation results are consistent with those of ref. 5. However, since that study used the Metropolis dynamic [see their Eq. (3)], the velocities cannot be compared directly. For asymptotically low T, the velocity is completely determined by the kink density, $\langle n(11s) \rangle$. This is the regime in which the single-step and PNG models are expected to hold. Indeed, they emerge in the proper limits from our analytic approximation, as shown in Eqs. (14) and (15). For larger $H \leqslant 2J$ and $T \leqslant T_c$, other spin classes also contribute significantly to the interface velocity. In this parameter range we obtain good agreement between theory and simulation almost everywhere. This agreement includes the disappearance of the velocity anisotropy with increasing T and H.

Both the SOS approximation for the interface structure, and the assumption of uncorrelated step heights employed in the nonlinear-response approximation break down for stronger fields. While the NLI approximation for the interface velocities remains very satisfactory overall, the breakdown of these assumptions can be detected more clearly in the spin-class populations. The only detailed theories of the local structure of driven interfaces that we are aware of, are for much simpler SOS models than the unrestricted one studied here, such as the body-centered SOS (BCSOS) and restricted SOS (RSOS) models.[32] It would therefore be interesting to compare our mean-field approximation for the interface structure with MC simulations of the driven SOS interface, so that the complications arising from overhangs and bubbles can be avoided.[39]

In summary, the approximations presented here give results for the spin-class populations and propagation velocities of Ising interfaces driven by nonzero fields, which are exact in the asymptotic limits of low T and H, and which agree well with MC simulations almost everywhere, even for H near $2J$ and T near T_c. It is not clear whether the wide regime of applicability is an accident limited to two dimensions, and it would therefore be interesting to extend the approach to three dimensions as well.

ACKNOWLEDGMENTS

P. A. Rikvold dedicates this paper to Professor George Stell on his 65th birthday. His friendship, encouragement, and scientific guidance are deeply appreciated.

We acknowledge useful conversations with R. K. P. Zia, G. Korniss, and M. A. Novotny, and comments on the manuscript by G. Korniss, M. A. Novotny, G. Brown, and two anonymous referees. Parts of this work were performed at the Colorado Center for Chaos and Complexity, University of Colorado at Boulder; the Faculty of Integrated Human Studies, Kyoto University; and the Department of Physics, University of Texas at Austin. Hospitality and partial support extended to P.A.R. at these institutions are gratefully acknowledged. The research was supported in part by National Science Foundation Grants No. DMR-9634873 and DMR-9981815, and by Florida State University through the Center for Materials Research and Technology and the Supercomputer Computations Research Institute (U.S. Department of Energy Contract No. DE-FC05-85ER25000).

REFERENCES

1. G. Stell and P. A. Rikvold, Polydispersity in fluids, dispersions, and composites: Some theoretical results, *Chem. Eng. Commun.* **51**:233 (1987).
2. S. Torquato, Morphology and effective properties of disordered heterogeneous media, *Int. J. of Solids and Structures* **35**:385 (1998).
3. A.-L. Barabási and H. E. Stanley, *Fractal Concepts in Surface Growth* (Cambridge University Press, Cambridge, 1995).
4. P. Meakin, *Fractals, Scaling and Growth far from Equilibrium* (Cambridge University Press, Cambridge, 1998).
5. P. Devillard and H. Spohn, Kinetic shape of Ising clusters, *Europhys. Lett.* **17**:113 (1992).
6. H. Spohn, Interface motion in models with stochastic dynamics, *J. Stat. Phys.* **71**:1081 (1993).
7. V. A. Shneidman, K. A. Jackson, and K. M. Beatty, Non-equilibrium interface of a two-dimensional low-temperature crystal, *J. Crystal Growth* **212**:564 (2000). This very recent paper proposes a nonlinear, kinetic equation for the average growth velocity. A stationary growth velocity, expected to be valid for very low T and H, is numerically obtained. It should be interesting to compare the results of this approach with those of the single-step and PNG models, as well as with those of the present approach.
8. M. Kardar, G. Parisi, and Y.-C. Zhang, Dynamic scaling of growing interfaces, *Phys. Rev. Lett.* **56**:889 (1986).
9. I. M. Lifshitz, Kinetics of ordering during second-order phase transitions, *Sov. Phys. JETP* **15**:939 (1962) [*Zh. Eksp. Teor. Fiz.* **42**:1354 (1962)].
10. S. M. Allen and J. W. Cahn, A microscopic theory for antiphase boundary motion and its application to antiphase domain coarsening, *Acta Metall.* **27**:1085 (1979).
11. A. B. Bortz, M. H. Kalos, and J. L. Lebowitz, A new algorithm for Monte Carlo simulation of Ising spin systems, *J. Comput. Phys.* **17**:10 (1975).

12. M. A. Novotny, A new approach to an old algorithm for the simulation of Ising-like systems, *Computers in Physics* **9**:46 (1995).
13. M. A. Novotny, Monte Carlo with absorbing Markov chains: Fast local algorithms for slow dynamics, *Phys. Rev. Lett.* **74**:1 (1995); erratum **75**:1424 (1995).
14. W. K. Burton, N. Cabrera, and F. C. Frank, The growth of crystals and the equilibrium structure of their surfaces, *Phil. Trans. Roy. Soc. (London) Ser. A* **243**:299 (1951).
15. J. Krug, H. T. Dobbs, and S. Majaniemi, Adatom mobility for the solid-on-solid model, *Z. Phys. B* **97**:281 (1995). This paper considers *conserved* dynamics.
16. K. Kawasaki, in *Phase Transitions and Critical Phenomena*, Vol. 2, C. Domb and M. Green, eds. (Academic, London, 1972).
17. Ph. A. Martin, On the stochastic dynamics of Ising models, *J. Stat. Phys.* **16**:149 (1977).
18. V. A. Shneidman, K. A. Jackson, and K. M. Beatty, Nucleation and growth of a stable phase in an Ising-type system, *Phys. Rev. B* **59**:3579 (1999).
19. R. A. Ramos, P. A. Rikvold, and M. A. Novotny, Test of the Kolmogorov–Johnson–Mehl–Avrami picture of metastable decay in a model with microscopic dynamics, *Phys. Rev. B* **59**:9053 (1999).
20. H. Tomita and S. Miyashita, Statistical properties of the relaxation process of metastable states in the kinetic Ising model, *Phys. Rev. B* **46**:8886 (1992).
21. P. A. Rikvold, H. Tomita, S. Miyashita, and S. W. Sides, Metastable lifetimes in a kinetic Ising model: Dependence on field and system size, *Phys. Rev. E* **49**:5080 (1994).
22. H. L. Richards, S. W. Sides, M. A. Novotny, and P. A. Rikvold, Magnetization switching in nanoscale ferromagnetic grains: Description by a kinetic Ising model, *J. Magn. Magn. Mater.* **150**:37 (1995).
23. M. Kolesik, M. A. Novotny, P. A. Rikvold, and D. M. Townsley, Projected dynamics for metastable decay in Ising models, in *Computer Simulation Studies in Condensed Matter Physics X*, D. P. Landau, K. K. Mon, and B. Schüttler, eds. (Springer-Verlag, Berlin, 1998), p. 246.
24. M. Kolesik, M. A. Novotny, and P. A. Rikvold, Projection method for statics and dynamics of lattice spin systems, *Phys. Rev. Lett.* **80**:3384 (1998).
25. M. A. Novotny, P. A. Rikvold, M. Kolesik, D. M. Townsley, and R. A. Ramos, Simulations of metastable decay in two- and three-dimensional models with microscopic dynamics, *J. Non-Cryst. Solids*, in press. E-print cond-mat/9909364.
26. H. N. V. Temperley, Statistical mechanics and the partition of numbers. II. The form of crystal surfaces, *Proc. Cambridge Phil. Soc.* **48**:683 (1952).
27. J. E. Avron, H. van Beijeren, L. S. Schulman, and R. K. P. Zia, Roughening transition, surface tension and equilibrium droplet shape in a two-dimensional Ising system, *J. Phys. A* **15**:L81 (1982).
28. P. Meakin, P. Ramanlal, L. M. Sander, and R. C. Ball, Ballistic deposition on surfaces, *Phys. Rev. A* **34**:5091 (1986).
29. M. Plischke, Z. Rácz, and D. Liu, Time-reversal invariance and universality of two-dimensional growth models, *Phys. Rev. B* **35**:3485 (1987).
30. J. Krug and H. Spohn, Anomalous fluctuations in the driven and damped sine-Gordon chain, *Europhys. Lett.* **8**:219 (1989).
31. J. Kertész and D. E. Wolf, Anomalous roughening in growth processes, *Phys. Rev. Lett.* **62**:2571 (1989).
32. J. Neergaard and M. den Nijs, Stationary-state skewness in KPZ-type growth, *J. Phys. A* **30**:1935 (1997).
33. G. Korniss, Z. Toroczkai, M. A. Novotny, and P. A. Rikvold, From massively parallel algorithms and fluctuating time horizons to non-equilibrium surface growth, *Phys. Rev. Lett.* **84**:1351 (2000).

34. M. Kotrla and A. C. Levi, Kinetic six-vertex model as model of bcc crystal growth, *J. Stat. Phys.* **64**:579 (1991).
35. J. Marro and R. Dickman, *Nonequilibrium Phase Transitions in Lattice Models* (Cambridge University Press, Cambridge, 1999), Chap. 7.
36. D. Dhar, Asymptotic shape of Eden clusters, in *On Growth and Form: Fractal and Non-Fractal Patterns in Physics*, H. E. Stanley and N. Ostrowsky, eds. (Martinus Nijhoff, Dordrecht, 1986), p. 288.
37. P. Meakin, R. Jullien, and R. Botet, Large-scale numerical investigation of the surface of Eden clusters, *Europhys. Lett.* **1**:609 (1986).
38. R. Hirsch and D. E. Wolf, Anisotropy and scaling of Eden clusters in two and three dimensions, *J. Phys. A* **19**:L251 (1986).
39. P. A. Rikvold and M. Kolesik, in preparation.